Spiral Intensity Patterns in the Internally Pumped Optical Parametric Oscillator

P. Lodahl and M. Bache*

Optics and Fluid Dynamics Department, Risø National Laboratory, Postbox 49, DK-4000 Roskilde, Denmark

M. Saffman

Department of Physics, University of Wisconsin, 1150 University Avenue, Madison, Wisconsin 53706

(Received 18 July 2000)

We describe a nonlinear optical system that supports spiral pattern solutions in the field intensity. This new spatial structure is found to bifurcate above a secondary instability in the internally pumped optical parametric oscillator. The analytical predictions of threshold and spatial scale for the instability are supplemented by detailed numerical investigations of the formation of spiral patterns.

PACS numbers: 42.65.Sf, 05.45.Yv, 42.65.Ky

The formation of spiral waves has been reported in many dynamical nonlinear systems including hydrodynamical convection, chemical reactions and optical processes [1]. In chemical and hydrodynamical processes spiral waves are observed in the field amplitude, as evident, e.g., in the Belousov-Zhabotinsky reactions [2]. In contrast, optical spiral waves generally appear in the phase structure of the optical field. These vortical structures are zeros of the optical intensity with a phase circulation around the vortex that is an integer multiplum of 2π, and they have been found in both linear and nonlinear optical systems [3–6]. They have been shown to be generic to the Maxwell-Bloch laser equations [5] and in reduced descriptions based on Ginzburg-Landau models that are used to approximate the laser behavior close to threshold [6]. Vortex structures have been observed experimentally in a range of laser oscillators [7,8].

The question arises if spiral structures in the field amplitude, analogous to those seen in chemical and hydrodynamic systems, also can be found in optics. Such amplitude spirals were observed in Ref. [9] using a specially designed nonlinear optical system with both diffusive interactions as well as nonlocal feedback. We show here that spiral intensity structures are also present in a standard and widely studied nonlinear optical system: an intracavity $\chi^{(2)}$ mediated quadratic nonlinear interaction. Intensity spirals are shown to appear above a secondary instability in the system, and are investigated through stability analysis and numerical simulations. The intensity spirals are fundamentally different from the phase spirals found in the laser case, and are found to originate from an amplitude instability in the system.

Studies of transverse pattern formation in $\chi^{(2)}$ cavity based processes were initiated with the optical parametric oscillator (OPO) in both the degenerate [10] and nondegenerate [11,12] configurations. Recently, interest was directed towards second harmonic generation (SHG) [13]. We have been concerned with the combined system consisting of second harmonic generation in the presence of a competing parametric process [14,15], also termed the internally pumped optical parametric oscillator (IPOPO). Apart from being an experimentally relevant system [16] the IPOPO also shows new features compared to the isolated SHG and OPO processes. Indeed, we demonstrate here that intensity spiral patterns can be found in the IPOPO. An equivalent analysis of the ordinary externally pumped nondegenerate OPO suggests that it does not support intensity spirals. Note that phase spiral solutions can, however, be found in the nondegenerate OPO [17].

The scaled cavity mean-field equations for the IPOPO with the fundamental A_1, second harmonic A_2, and two nondegenerate parametric fields $A_\pm$ resonant are given by [15]

$$\frac{\partial A_1}{\partial t} = (-1 + i\Delta_1)A_1 + iA_1^* A_2 + i\nabla_\perp^2 A_1 + E, \quad (1)$$

$$\frac{\partial A_2}{\partial t} = (-\gamma + i\Delta_2)A_2 + iA_1^2 + 2iA_+A_- + \frac{i}{2}\nabla_\perp^2 A_2, \quad (2)$$

$$\frac{\partial A_+}{\partial t} = (-1 + i\Delta_+)A_+ + iA_-^* A_2 + i\nabla_\perp^2 A_+, \quad (3)$$

$$\frac{\partial A_-}{\partial t} = (-1 + i\Delta_-)A_- + iA_+^* A_2 + i\nabla_\perp^2 A_-. \quad (4)$$

Here Δ_j, $j = 1, 2, +, -$, are cavity detunings of the four fields while γ is the ratio between the loss rate of the second harmonic and the fundamental. Diffraction is included through the terms containing the transverse Laplacian while the cavity is pumped at the fundamental frequency with an amplitude E. The mutual influence of the two $\chi^{(2)}$ processes regarding pattern formation was investigated previously [15]. There the main focus was on the situation where the SHG instabilities are encountered below the parametric threshold. In the opposite case, where the parametric process sets in below the SHG instabilities, it is possible to derive exact analytical solutions valid above threshold for the parametric process. This was previously done by Marte [18] for the IPOPO in the absence of diffraction. With diffraction the solutions are of the form $A_1 = \overline{A}_1$, $A_2 = \overline{A}_2$, $A_\pm = \overline{A}\exp(\pm i\mathbf{k}_\perp \cdot \mathbf{r})$; i.e., the parametric fields are in general emitted off-axis in

 0031-9007/00/85(21)/4506(4)$15.00

the cavity while the fundamental and second harmonic are on-axis homogeneous solutions. Substituting the solutions into Eqs. (1)–(4), the amplitudes are found to obey

$$|\overline{A}_1|^2 = \zeta_1(E^2) - \zeta_2|\overline{A}|^2, \tag{5}$$

$$|\overline{A}_2|^2 = \delta(k_\perp^2), \tag{6}$$

$$|\overline{A}|^4 + \zeta_3|\overline{A}|^2 + \zeta_4 = \frac{1}{4}|\overline{A}_1|^4, \tag{7}$$

where we have introduced the coefficients

$$\zeta_1(E^2) = \frac{E^2 - 2\delta(k_\perp^2)(\gamma - \Delta_1\Delta_2)}{1 + \Delta_1^2 + \delta(k_\perp^2)}, \tag{8}$$

$$\zeta_2 = \frac{4\sqrt{\delta(k_\perp^2)}}{1 + \Delta_1^2 + \delta(k_\perp^2)}[\cos\phi(k_\perp^2) + \Delta_1 \sin\phi(k_\perp^2)], \tag{9}$$

$$\zeta_3 = \sqrt{\delta(k_\perp^2)}[\gamma\cos\phi(k_\perp^2) - \Delta_2 \sin\phi(k_\perp^2)], \tag{10}$$

$$\zeta_4 = \frac{1}{4}\delta(k_\perp^2)(\gamma^2 + \Delta_2^2), \tag{11}$$

and all the dependence on the transverse wave number $k_\perp$ is in the parameters $\delta(k_\perp^2) = 1 + (\Delta_1 - k_\perp^2)^2$, $\phi(k_\perp^2) = \arctan(\Delta_1 - k_\perp^2)$. In the above analysis we have let $\Delta_+ = \Delta_- = \Delta_1$, which is a consequence of energy conservation and a symmetry argument, as discussed in [19].

Two fundamentally different regions exist depending on the sign of the fundamental detuning Δ_1. For $\Delta_1 > 0$, the parametric solutions with $k_\perp = \sqrt{\Delta_1}$ are always linearly stable [19]. Consequently all the instabilities otherwise obtained from the SHG process are completely quenched by the parametric process.

Here we consider the case of negative detuning of the fundamental. In this case all the SHG instabilities can be excited since by varying Δ_2 they can appear with lowest threshold (cf. Fig. 2 in Ref. [15]). Furthermore, a region exists where the parametric threshold is lowest and the exact solutions discussed above can be excited, where in this case the fields are emitted on-axis with $k_\perp = 0$. As opposed to the off-axis solutions that appear for positive fundamental detuning, the on-axis solutions can destabilize leading to a secondary instability in the IPOPO system. This instability is investigated by perturbing the solutions according to $A_j = \overline{A}_j + \delta A_j \exp(\Lambda t + i\mathbf{K}_\perp \cdot \mathbf{r}) + \delta B_j \exp(\Lambda^* t - i\mathbf{K}_\perp \cdot \mathbf{r})$, $j = 1, 2, +, -$, and by performing a linear stability analysis for the perturbation amplitudes δA_j, δB_j. This leads to an 8×8 matrix equation for the eigenvalue Λ. The onset of the instability can be found by plotting the growth rates $\mathrm{Re}(\Lambda_{\max})$, i.e., the largest real part of the eight eigenvalues. The imaginary part of the critical eigenvalue is nonvanishing at threshold which means the instability is oscillatory.

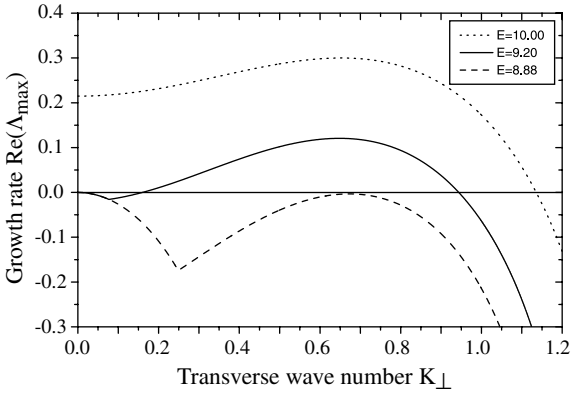

FIG. 1. Growth rates $\mathrm{Re}(\Lambda_{\max})$ for the secondary instability as a function of the transverse wave number $K_\perp$, with $\Delta_1 = -2.5$, $\Delta_2 = 0.3$, $\gamma = 1$, and for three different values of E.

An example of growth rates for the secondary instability is displayed in Fig. 1 for three values of the pump field E. The instability threshold is found to be $E_t \simeq 8.88$ and sets in at the critical transverse wave number $K_c \simeq 0.68$ which determines the spatial scale of the pattern. Above threshold the growth rates are peaked near K_c and vanish at $K_\perp = 0$ resembling a class II instability according to the classification given in [1]. Increasing the pump, the growth rates are found to be positive in a rather broad band ranging to $K_\perp = 0$. This is in contrast to the pattern forming instabilities otherwise found in the IPOPO [15,19], where positive growth rates near threshold are obtained only in a narrow peaked band around the critical wave number K_c (class I instability). The broadband instability is expected to lead to different dynamics. Hence the amplitude equation that can be used to describe generic pattern formation close to threshold has been shown to be of the Kuramoto-Sivashinsky type for class II instabilities as opposed to the more common Newell-Whitehead-Segel models for class I instabilities [1]. This outlines the reason for expecting new spatiotemporal dynamics from the secondary parametric instability. The emergence of spiral structures is not unexpected due to the analogous behavior of the complex Ginzburg-Landau equation where the phase of the exact solutions is found to obey a Kuramoto-Sivashinsky equation and destabilize to spirals [1].

Numerical integration of Eqs. (1)–(4) is undertaken in order to investigate the formation of spatial structures above threshold. The numerical method utilizes a Fourier split-step routine with periodic boundary conditions. Figure 2 shows the formation of a traveling roll pattern for $E = 9.2$ and the parameters given in Fig. 1. The simulation is seeded with random noise at $t = 0$ that gradually develops into the periodic modulated structure observed at $t = 3000$. The spatial scale of the roll pattern is found to be $K_\perp \simeq 0.81$ in reasonable agreement with the threshold value $K_c \simeq 0.68$ predicted from the stability analysis. It is worth mentioning that a traveling wave instability was already found in the IPOPO [15];

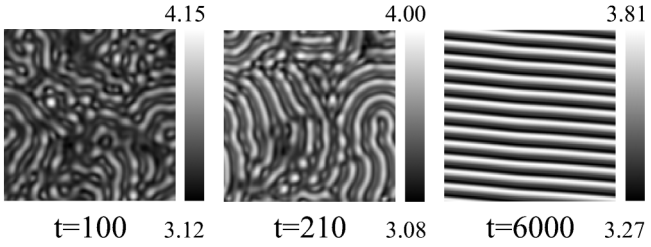

FIG. 2. Example of formation of a traveling roll pattern in the near-field image of $|A_1|^2$ starting from random noise at $t = 0$. The pump amplitude is $E = 9.2$ and other parameters are as in Fig. 1. The window size is 96.7×96.7.

however, this was due to an SHG instability while the secondary parametric instability mechanism reported here is fundamentally different.

For other parameters positive growth rates extend to $K_\perp = 0$ and here intensity spiral patterns can be obtained from the secondary instability. An example is presented in Fig. 3. Starting from initial random noise, a grainy structure is formed ($t = 222$) that gradually emerges into modulated wave fronts reminiscent of the traveling rolls ($t = 500$). They curve to form spiral structures that in general are found to become more and more regular and increase in size. The spirals rotate in time at the Hopf frequency given by the imaginary part of the eigenvalues found in the stability analysis. Similar structures are observed in the near field of all four cavity fields.

Figure 4 shows the broad band of positive growth rates present in the case where spirals are formed. The instability threshold is found to be $E_t \simeq 6.61$ and above that positive growth rates are obtained in an interval starting at $K_\perp = 0$ and ranging up to about $K_\perp \simeq 0.7$–0.8. The growth rates are weakly peaked around $K_\perp \simeq 0.4$ which determines the spatial scale of the modulated structure. Spiral patterns can be found for both $E = 6.8$ and $E = 7.0$, and in general for parameters that give positive growth rates in a broad weakly peaked band ranging to $K_\perp = 0$. In contrast, when the peaked growth rates vanish at zero, as in the case of $E = 9.2$ in Fig. 1, the traveling rolls are found. Increasing the pump, however, these rolls destabilize to spirals as also expected from the behavior of the growth rates for $E = 10$ in Fig. 1.

Although the spirals can be formed directly from random noise without formation of a fully developed traveling roll pattern, it is clear that the underlying roll structure

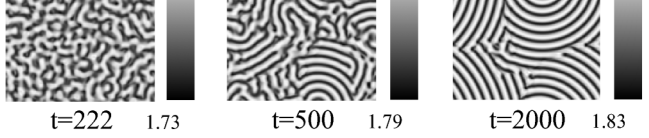

FIG. 3. Time evolution showing the formation of spiral patterns in $|A_1|^2$ for $E = 7.0$, $\Delta_1 = -2.5$, $\Delta_2 = -0.7$, $\gamma = 1$, and a window size of 200×200.

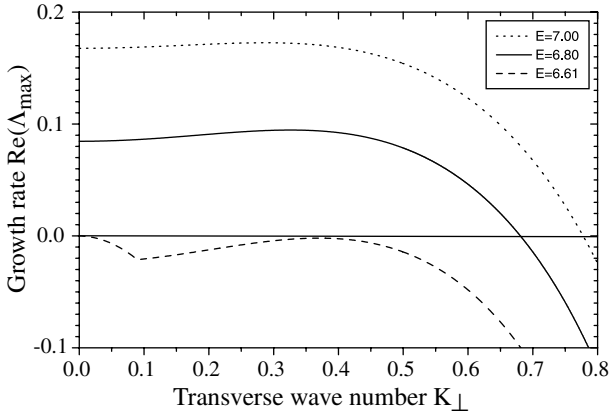

FIG. 4. Growth rates for three different values of the pump E and otherwise the same parameters as in Fig. 3.

plays an essential role. Hence it is of interest to study the formation of intensity spiral patterns from defect induced destabilization of the traveling rolls. This is investigated by performing a numerical simulation starting with a roll pattern generated with $E = 9.2$ corresponding to the one seen in Fig. 2. At $t = 0$ the pump level is abruptly increased to $E = 10$ where spirals are expected and the time series in Fig. 5 shows the destabilization of the roll and gradual formation of spirals displayed both in the near field and in the far field. The near-field pictures show clearly how defects truncate the ideal roll pattern that subsequently curves into spirals. The far-field pictures give an indication of the wave numbers contributing to the formation of spirals. Thus, as anticipated from the growth rates, a wide band of wave numbers become excited including the ones close to $K_\perp = 0$. For the fully developed spirals ($t = 2000$) the far-field picture constitutes a ring since k vectors along all directions contribute to the spiral pattern.

In order to test the robustness of the spiral structures and their dependence on the boundary conditions we have also performed simulations with a localized

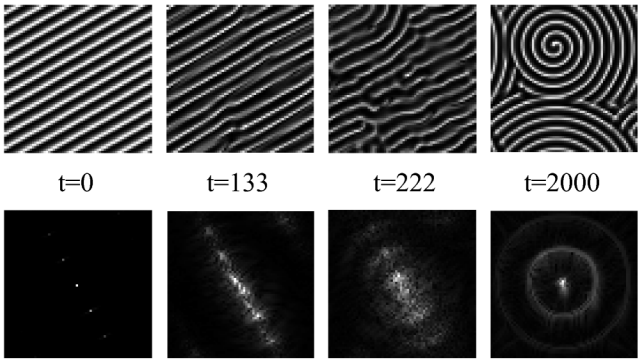

FIG. 5. Time series showing the formation of spirals due to destabilization of a traveling roll pattern. The plots show the parametric intensity, $|A_+|^2$, both in the near field (upper row) and in the far field (lower row). The system parameters and box size are as in Fig. 2 while the pump level is increased to $E = 10$ at $t = 0$.

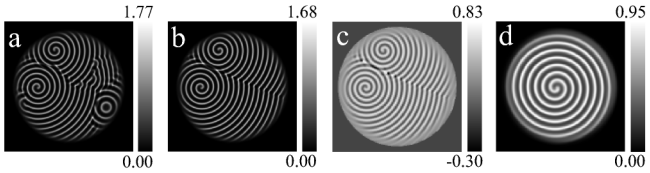

FIG. 6. Numerical simulations performed with super-Gaussian pump beam. (a) ($t = 1000$) and (b), (c) ($t = 2000$) are obtained for the same parameters as in Fig. 3 and with a box size of 300×300, while (d) is done with parameters corresponding to Fig. 2 and a box size of 150×150. Frames (a), (b), (d) show the intensity distribution of one of the parametric fields, while frame (c) shows the phase structure of (b).

super-Gaussian pump beam which defines the boundaries. Figure 6a shows that spirals exist also in that case. Interestingly, a target defect is also observed but due to interaction with the waves emitted by the spiral the target is subsequently annihilated after longer integration times as shown in Fig. 6b. As shown in Fig. 6c there is also a spiral structure in the phase of the field, although the total variation is much less than 2π and there is no singularity at the center. While the spirals appear not so sensitive to the boundary conditions, this turns out to be the case for the traveling rolls. Thus, performing a simulation with localized pump and otherwise the same parameters as in Fig. 2, a large spiral structure is formed (Fig. 6d) that reflects the circular symmetry of the boundaries. Similar boundary induced structures have been reported for the Maxwell-Bloch equations [20].

A natural point to investigate is the possible existence of intensity spirals also in the ordinary OPO where the pump term is in the second harmonic. For the nondegenerate OPO exact solutions analogous to Eqs. (5)–(11) for the IPOPO exist and were given by Longhi [12]. A stability analysis of the solutions reveals a secondary instability in the case of negative parametric detuning. Although the growth rates indicate a class II instability, spiral structures could not be found numerically. Indeed, the dynamics was found to be rather different since the traveling rolls were also absent and instead square intensity patterns were regularly observed.

In conclusion, we have demonstrated the existence of intensity spiral patterns in an optical IPOPO system. Perturbation analysis revealed a secondary instability in the system above which the spirals were formed. A detailed numerical analysis was carried out including a study of the spiral forming mechanism and the dependence on boundary conditions. Finally, the IPOPO was compared to the ordinary pumped OPO where spirals could not be found.

P. L. and M. B. acknowledge financial support from the Danish Research Academy.

Note added.—Intensity spirals similar to those described here were observed recently in an optical experiment with atomic nonlinearity [21].

*Also at IMM, The Technical University of Denmark, Dk-2800 Lyngby, Denmark.

[1] M. C. Cross and P. C. Hohenberg, Rev. Mod. Phys. **65**, 851 (1993); Y. Kuramoto, *Chemical Oscillations, Waves, and Turbulence* (Springer-Verlag, Berlin, 1984).
[2] A. Zaikin and A. Zhabotinsky, Nature (London) **225**, 535 (1970); A. T. Winfree, Science **175**, 634 (1972).
[3] For a collection of recent reviews see *Optical Vortices,* edited by M. Vasnetsov and K. Staliunas (Nova Science Publishers, Inc., Commack, 1999).
[4] N. B. Baranova, B. Ya. Zel'dovich, A. V. Mamaev, N. F. Pilipetsky, and V. V. Shkunov, Pis'ma Zh. Eksp. Teor. Fiz. **33**, 206 (1981) [JETP Lett. **33**, 195 (1981)].
[5] P. Coullet, L. Gil, and F. Rocca, Opt. Commun. **73**, 403 (1989); D. Yu, W. Lu, and R. G. Harrison, Phys. Rev. Lett. **77**, 5051 (1996).
[6] L. Gil, Phys. Rev. Lett. **70**, 162 (1993).
[7] C. O. Weiss, Phys. Rep. **219**, 311 (1992).
[8] F. T. Arecchi, G. Giacomelli, P. L. Ramazza, and S. Residori, Phys. Rev. Lett. **67**, 3749 (1991).
[9] S. A. Akhmanov, M. A. Vorontsov, and V. Yu. Ivanov, Pis'ma Zh. Eksp. Teor. Fiz. **47**, 611 (1988) [JETP Lett. **47**, 707 (1988)].
[10] G.-L. Oppo, M. Brambilla, and L. A. Lugiato, Phys. Rev. A **49**, 2028 (1994); G. J. de Valcárcel, K. Staliunas, E. Roldán, and V. J. Sánchez-Morcillo, Phys. Rev. A **54**, 1609 (1996).
[11] G.-L. Oppo, M. Brambilla, D. Camesasca, A. Gatti, and L. A. Lugiato, J. Mod. Opt. **41**, 1151 (1994).
[12] S. Longhi, Phys. Rev. A **53**, 4488 (1996).
[13] C. Etrich, U. Peschel, and F. Lederer, Phys. Rev. Lett. **79**, 2454 (1997); Phys. Rev. E **56**, 4803 (1997); S. Longhi, Opt. Lett. **23**, 346 (1998).
[14] P. Lodahl and M. Saffman, Phys. Rev. A **60**, 3251 (1999).
[15] P. Lodahl, M. Bache, and M. Saffman, Opt. Lett. **25**, 654 (2000).
[16] S. Schiller and R. L. Byer, J. Opt. Soc. Am. B **10**, 1696 (1993).
[17] K. Staliunas, Opt. Commun. **91**, 82 (1992).
[18] M. A. M. Marte, Phys. Rev. A **49**, R3166 (1994).
[19] P. Lodahl, M. Bache, and M. Saffman, Phys. Rev. A (to be published).
[20] I. Aranson, D. Hochheiser, and J. V. Moloney, Phys. Rev. A **55**, 3173 (1997).
[21] B. Schäpers, M. Feldmann, T. Ackemann, and W. Lange, in *Nonlinear Guided Waves and Their Applications,* OSA Technical Digest (Optical Society of America, Washington, DC, 1999), p. 44.